



## Article

# Identification of Immune Function-Related Subtypes in Cutaneous Melanoma

Lin Liu <sup>†</sup>, Junkai Zhu <sup>†</sup>, Tong Jin, Mengjia Huang, Yi Chen, Li Xu , Wenxuan Chen, Bo Jiang <sup>\*</sup> and Fangrong Yan <sup>\*</sup> 

Research Center of Biostatistics and Computational Pharmacy, China Pharmaceutical University, Nanjing 210009, China; linliu.cpu@foxmail.com (L.L.); zhujunkai97@126.com (J.Z.); tjin.cpu@foxmail.com (T.J.); chung\_hmj@163.com (M.H.); yichencheny@163.com (Y.C.); 3320051716@stu.cpu.edu.cn (L.X.); chengwenxuan1997@outlook.com (W.C.)

<sup>\*</sup> Correspondence: jiangbo@cpu.edu.cn (B.J.); yanfangrong@cpu.edu.cn (F.Y.)

<sup>†</sup> These authors contributed equally.

**Abstract:** Tumour immunotherapy combined with molecular typing is a new therapy to help select patients. However, molecular typing algorithms related to tumour immune function have not been thoroughly explored. We herein proposed a single sample immune signature network (SING) method to identify new immune function-related subtypes of cutaneous melanoma of the skin. A sample-specific network and tumour microenvironment were constructed based on the immune annotation of cutaneous melanoma samples. Then, the differences and heterogeneity of immune function among different subtypes were analysed and verified. A total of 327 cases of cutaneous melanoma were divided into normal and immune classes; the immune class had more immune enrichment characteristics. After further subdividing the 327 cases into three immune-related subtypes, the degree of immune enrichment in the “high immune subtype” was greater than that in other subtypes. Similar results were validated in both tumour samples and cell lines. Sample-specific networks and the tumour microenvironment based on immune annotation contribute to the mining of cutaneous melanoma immune function-related subtypes. Mutations in *B2M* and *PTEN* are considered potential therapeutic targets that can improve the immune response. Patients with a high immune subtype can generally obtain a better immune prognosis effect, and the prognosis may be improved when combined with TGF- $\beta$  inhibitors.

**Keywords:** cutaneous melanoma; therapeutic targets; immune function-related subtype; immunotherapy



**Citation:** Liu, L.; Zhu, J.; Jin, T.; Huang, M.; Chen, Y.; Xu, L.; Chen, W.; Jiang, B.; Yan, F. Identification of Immune Function-Related Subtypes in Cutaneous Melanoma. *Life* **2021**, *11*, 925. <https://doi.org/10.3390/life11090925>

Academic Editors: Attila Gabor Szollosi and Magdolna Szanto

Received: 10 August 2021

Accepted: 30 August 2021

Published: 6 September 2021

**Publisher's Note:** MDPI stays neutral with regard to jurisdictional claims in published maps and institutional affiliations.



**Copyright:** © 2021 by the authors. Licensee MDPI, Basel, Switzerland. This article is an open access article distributed under the terms and conditions of the Creative Commons Attribution (CC BY) license (<https://creativecommons.org/licenses/by/4.0/>).

## 1. Introduction

Cancer is not a single disease but a collection of multiple biological entities, and each has its own molecular characteristics and clinical significance [1]. Traditionally, cancer classification was based on histopathology and clinical characteristics, most of which depend on clinicians' judgement. However, studies show that prognosis and treatment responses vary between cancer subtypes and within subtypes. Therefore, it is necessary to develop methods that can accurately predict the key results of individual patients [2,3]. Although some progress has been made in the field, there are still unexplained inter-tumoural heterogeneities leading to varying survival outcomes and differences in treatment responses [4]. Gene expression features are easy to measure from tissue samples, and may be used to identify personalized “driving mutations” [5], differentially expressed genes and pathways [6], and personalized gene networks [7]. Although genes have been successfully used as biomarkers for cancer diagnosis [8], it is not clear whether gene biomarkers are the most suitable method for treatment indicator classification. Conversely, it may be more meaningful to describe diseases by using system-specific dysfunction rather than the dysfunction [9,10] of individual molecules, which is based on the gene regulatory network.

Currently, intergenic relationships can be obtained in three ways: (1) gene regulation networks based on existing public database information; (2) gene regulation network based on intergenic correlation [11] or causality inferred [12]; and (3) gene regulation network based on an annotated database by prior information combined with gene expression data [13], which is called a mixed method. Most of the existing studies build networks based on information from all samples. In 2007, Borgwardt et al. [14] proposed using the PPI network as a reference network template, and the edges were tailored according to the gene co-expression state of the individual relative to the whole population. In 2009, Kuijjer et al. [15] further proposed the LIONESS method, which constructs personalized networks by evaluating the contribution of each sample to gene regulatory networks. The two methods have a common disadvantage: when a new sample enters the network, all network information needs to be recalculated. In 2019, Thin Nguyen et al. [16] proposed a new method to construct a sample-specific network called the “personalized annotation-based networks” (PAN). This method uses an annotated database information to transform gene expression data into a network, where nodes correspond to functional terms and edges correspond to the correlation between points. Since PAN considers a single sample that discards common information between samples, it can effectively avoid the defects of recalculation.

As a representative immunotherapy, cutaneous melanoma (SKCM) has a high mortality rate given its high malignancy, high incidence, and easy metastasis [17]. At present, immunotherapy is effective in the treatment of skin melanoma, but its disadvantages, such as low response rate, significant differences in immune response in different patients and unexpected adverse reaction occurrence, make it less effective [18,19]. Therefore, how to select patients suitable for immunotherapy is an urgent issue [20]. As molecular typing based on immune function can identify the specific biological characteristics of the population to adapt to specific treatments [21], it is an effective means to improve the efficacy of SKCM immunotherapy. However, the relationship between SKCM subtypes and immune function has not been well explored.

Here, we comprehensively analysed the molecular profiles of SKCM, including omics characteristics, immune mechanisms, and stromal cell infiltration abundance based on sample-specific networks, to identify subtypes related to immune function in SKCM and the molecular characteristics behind their subtypes.

## 2. Materials and Methods

### 2.1. Patients and Samples

The discovery cohort used in this study was from The Cancer Genome Atlas (TCGA) under the SKCM archive with a total of 327 tumour samples; gene expression, mutation, DNA methylation, and clinical data were retrieved. An external validation cohort including 214 SKCM data and paracancerous tissues was obtained from the GEO database (GSE7553 [22] [ $n = 82$ ], GSE23376 [23] [ $n = 22$ ], GSE19234 [24] [ $n = 44$ ], GSE15605 [25] [ $n = 58$ ]), and 206 tumour samples (Supplementary Table S1) were merged based on elimination of batch effects. Immune annotation information was obtained from the MSigDB database. The data of cell lines [26] ( $n = 49$ ) in cutaneous melanoma were downloaded from DepMap (<https://depmap.org/portal/>, accessed on 9 August 2021).

### 2.2. Sample-Specific Networks Were Constructed with the SING Method

We selected the C7 data set in the MSigDB database as the annotated database and the modified PAN method as SING (single sample immune signature network), which followed the analytic process below (Figure 1).

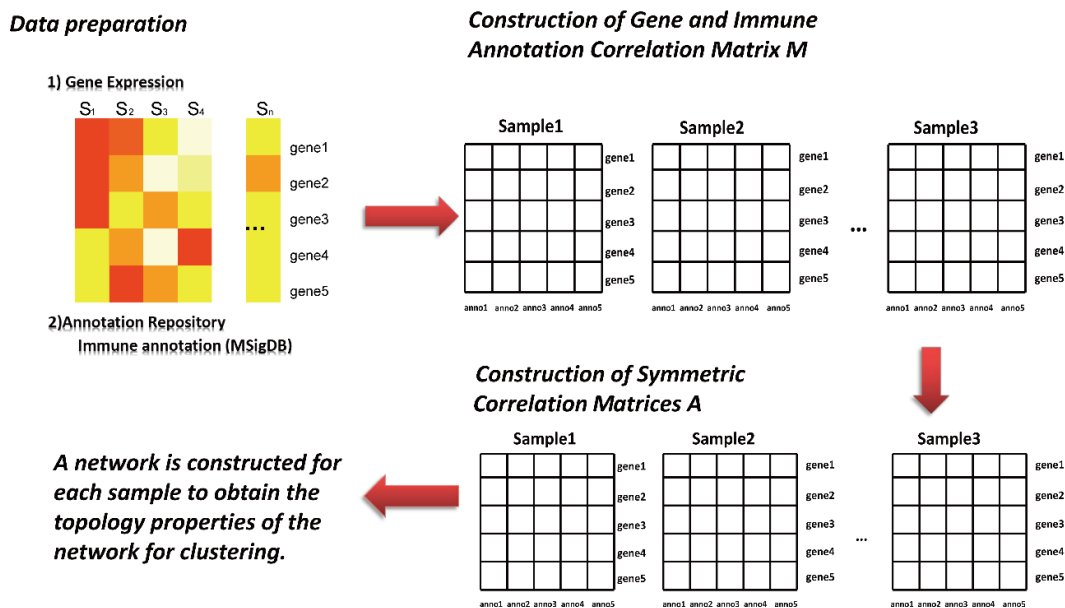


**Figure 1.** Flowchart of Sample Specific Network Algorithm. (1) Prepare data for feature selection. (2) Construct the gene and immune annotation correlation matrix. (3) Build a sample-specific network. (4) Compute network topology information.

Feature selection

- (1) The high-dimensional nature of gene expression data makes it necessary to reduce dimensionality before analysis. For each gene data set, the top 500 genes were selected according to the order of their total variance and included in subsequent analysis and calculation.
- (2) Construction of gene and immune annotation correlation matrix
- (3)  $M_{p,q}^j$  is the correlation matrix between the gene and immune annotation, in which  $j$  corresponds to the  $j$  sample,  $p$  corresponds to the first gene, and  $q$  corresponds to the first annotation information in the immune annotation database. The corresponding element in the matrix (line  $p$ , column  $q$ ) is the expression value of  $p$ ; otherwise, it is recorded as 0.
- (4) Development of sample-specific network
- (5) The symmetric correlation matrix  $A_{p,q}^j$  is further generated by the matrix  $M_{p,q}^j$ . Each element in the matrix corresponds to the Euclidean distance between two annotation pieces of information  $q$  and  $q^*$ . Afterward, to transform into a discrete network, this study further selected the edge of the top 10% weight in the symmetric correlation matrix  $A_{p,q}^j$  to construct the adjacency matrix.
- (6) Computing network topology information.

Once the discrete network construction of each sample was completed, the topological property “degree” of the network was calculated and obtained for subsequent clustering analysis. For a given sample  $S$ , its network is represented as  $G^S(V^S, E^S)$ , and the corresponding topological property is denoted as  $h^S$ , which is a vector,  $h^S = [h_1^S, \dots, h_{|V^S|}^S]$

$$E(v_j^s, v_k^s) = \begin{cases} 1, & \text{if } j \text{ is connected with } k \\ 0, & \text{otherwise} \end{cases}$$

$$h_j^s = \sum_{v_k^s \in V^s - \{v_j^s\}} l(v_j^s, v_k^s)$$

### 2.3. Clustering Algorithm

Clustering is an effective algorithm for molecular typing and has been successfully applied in the molecular typing of many kinds of cancer [1,27]. We used a model-based clustering algorithm based on the Gaussian finite mixture model (R package “mclust” v5.4.7) to find the best cluster numbers of the SKCM subtypes. For cancer subtype classification, we used hierarchical clustering and K-means algorithms. In the validation cohort, supervised consensus clustering was used to verify the existence of immune subtypes. The gene expression profile was resampled 500 times. In each resampling, 80% of the samples and 80% of the genes in the original matrix were taken. During each clustering process, the distance was measured by the 1-Pearson correlation coefficient, and the linkage was set as error sum of square (ESS) between classes.

### 2.4. Assessment of Immune and Stromal Cell Infiltration

As the degree of infiltration is related to the prognosis of immunotherapy in immune and stromal cells, we used the R package “MCPcounter” (v1.2.0) [28] to calculate the abundance fraction of eight immune cells (T cells, CD8 + T cells, NK cells, cytotoxic lymphocytes, B cell lineages, single-cell lineage cells, myeloid dendritic cells, and neutrophils) in the tumour microenvironment and two stromal cells (endothelial cells and fibroblasts). Then, “xCell” (v1.1) [29] was used to calculate 64 immune and nonimmune cell types, and “ESTIMATE” (v1.0.13) [30] was used to calculate the immune cell and stromal cell infiltration score.

### 2.5. Cytolytic Activity

Cell dissolution activity, also known as cell killing activity, can be used to characterize the immunogenic nature [31] of tumours. We obtained the cytolytic activity by calculating the geometric mean of granzyme A (GZMA) and perforin 1 (PRF1) gene expression in each sample.

### 2.6. Gene Differential Expression Analysis

The standard analysis process of “DESeq” (v1.30.1) [32] was used to analyse the differential gene expression of the original count data obtained by RNA sequencing. Nominal  $p$  values were adjusted by the false discovery rate (FDR). Genes with fold change  $\geq 2$  and  $FDR < 0.05$  were considered differentially upregulated genes, while those with fold change  $\leq 1/2$  and  $FDR < 0.05$  were considered differentially downregulated genes.

### 2.7. Differential Gene Enrichment Analysis

The gene enrichment analysis included GO functional annotation and KEGG pathway analysis. The GO functional annotation was completed by the DAVID 6.8 [33,34] online database, and KEGG pathway analysis was performed by the R package “clusterProfiler” (v3.18.1) [35]. Single-sample gene set enrichment analysis (ssGSEA) was performed based on the R package “GSVA” (v1.38.2) [36] to obtain the enrichment fraction of the gene set in a single sample. The scores of 24 microenvironment cell types were calculated, and the final microenvironment cell abundance was further adjusted by tumour purity through the formula  $\text{score}/(1 - \text{tumor purity})$ .

### 2.8. Recognition of Cancer Mutation-Driven Genes and Calculation of Tumour Mutation Load (TMB)

Based on cancer somatic mutation data, we used the R package “MutSigCV” (v2.0) [37] to identify the significantly driving mutated genes of the subtypes ( $q < 0.05$ ). Then, “maftools” (v2.6.05) were used to calculate the TMB in each subtype [38] to reflect mutations in tumour cells.

### 2.9. DNA Methylation Differential Analysis

We analysed two methylation statuses of the promoter: (1) hypermethylation status and (2) demethylation status. First, low-quality probes were filtered and differentiated

CpG sites were identified. This result suggested that when  $\log_2\text{FoldChange} > 0$  and the adjusted  $p$  value  $< 0.01$ , the probe showed a hypermethylation level; when  $\log_2\text{FoldChange} < 0$  and the adjusted  $p$  value  $< 0.01$ , the probe showed a low methylation level (R package “ChAMP” v2.20.1) [39].

### 2.10. Survival Analyses

To confirm whether there was a significant difference in survival between subtypes, a Kaplan–Meier curve [40] was used for survival analysis and the log-rank test for detection of significant difference ( $p < 0.05$ ). Univariate Cox proportional hazards regression was used to calculate the predictors associated with cancer survival [41]. After integrating all predictors, the nomogram [42] was used to reflect the correlation between the variables in the prediction model. A multivariate Cox regression model according to the published literatures [43,44] was used to calculate the risk score, which showed prognostic value.

## 3. Results

### 3.1. Determination and Verification of Cluster Number

Based on the degree topological property matrix of immune annotation sample-specific as input matrix, the optimal number of clusters were tested from one to six. The sample data were divided into two categories (Figure 2A). Then, the hierarchical clustering algorithm where the distance was measured by 1-Pearson’s coefficient and the clustering method was set as ward. Finally, 146 samples fell into the first category, called the C1 class and 181 samples fell into the second category, called the C2 class.

To verify the validity of the clustering results, the two clustered categories were compared with the TCGA classification results. A high correlation was found between them, and the immune subclass mainly overlapped with the C2 class (Figure 2B). Furthermore, the two categories were compared with another published dataset (Figure 2C) that contained 47 patients with SKCM [45] who responded to immunotherapy. C2 may have a high likelihood of responding to anti-PD-1 therapy (Bonferroni corrected  $p = 0.008$ ). Then, univariate Cox regression was used to analyse those factors that may affect the survival of SKCM patients (Supplementary Table S2). Age at diagnosis, body weight, race, tumour stage, UV markers, UV rate, metastatic status, and ploidy were significantly associated with patient prognostic survival ( $p < 0.05$ ). The nomogram (Figure 2D) can predict the survival rate of patients at different factor levels.

### 3.2. Definition and Extraction of Immune Subtypes

To explore the immune characteristics in SKCM, we defined subtypes of C1 and C2 based on the immune and matrix score, infiltration abundance of immune and stromal cells, and cytopathic activity. As the C2 class was more immune-infiltrated, we defined the C1 class as the “normal class” and C2 as the “immune class”.

The optimal clustering number of the immune class was three according to the BIC value (Figure 3A). Based on the K-means clustering method, the number of samples for the three classes were 38, 133, and 10. Combining immune clustering with normal class (Supplementary Figure S1), “immune2 class” can be significantly separated from other classes. “Immune3 class” and “normal class” had high similarities in the tumour microenvironment. In addition, there was no significant difference in the degree of immune infiltration between the “normal class” and “immune3 class” (Supplementary Figure S2). The immune infiltration of the “immune1 class” and “immune2 class” were significantly different. Therefore, the “immune3 class” and “normal class” were combined as the “new-normal class” in this study. Comparing the tumour microenvironment and immune score of the three types (Figure 3B,C), we found significant differences among them. “xCell” was used to calculate the invasion abundance of tumour immune and stromal cells. Tumour immune infiltration in the “immune 2 class” was significantly higher than that in the other two subtypes (Figure 3D). A significant prognostic difference among them ( $p = 0.0039$ ) was

also observed: the “new-normal class” was the worst, followed by “immune1 class”, and “immune2 class” was the best (Figure 3E).

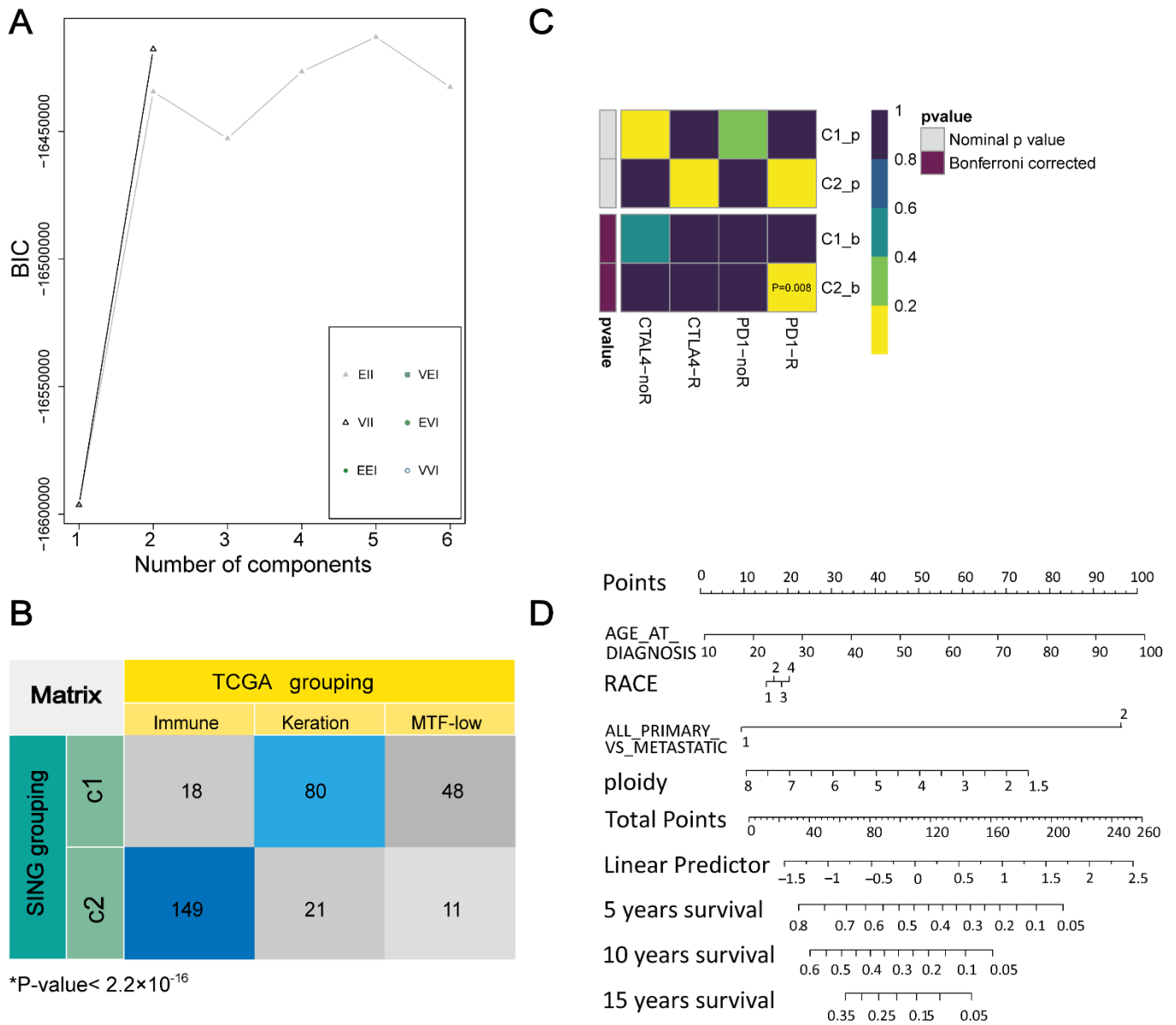


**Figure 2.** Define and validate the best SKCM cluster number. (A) Determination of the optimal cluster number ( $k = 2$ ) according to BIC values. (B) Comparing the two classes and TCGA classification, the “immune subclass” mainly overlapped with the C2 class ( $p < 2.2 \times 10^{-16}$ ). (C) Submap analysis showed that the C2 class may be more sensitive to programmed cell death protein 1 inhibitors (Bonferroni corrected  $p = 0.008$ ). (D) The nomogram directly reflected the correlation between variables in the prediction model.

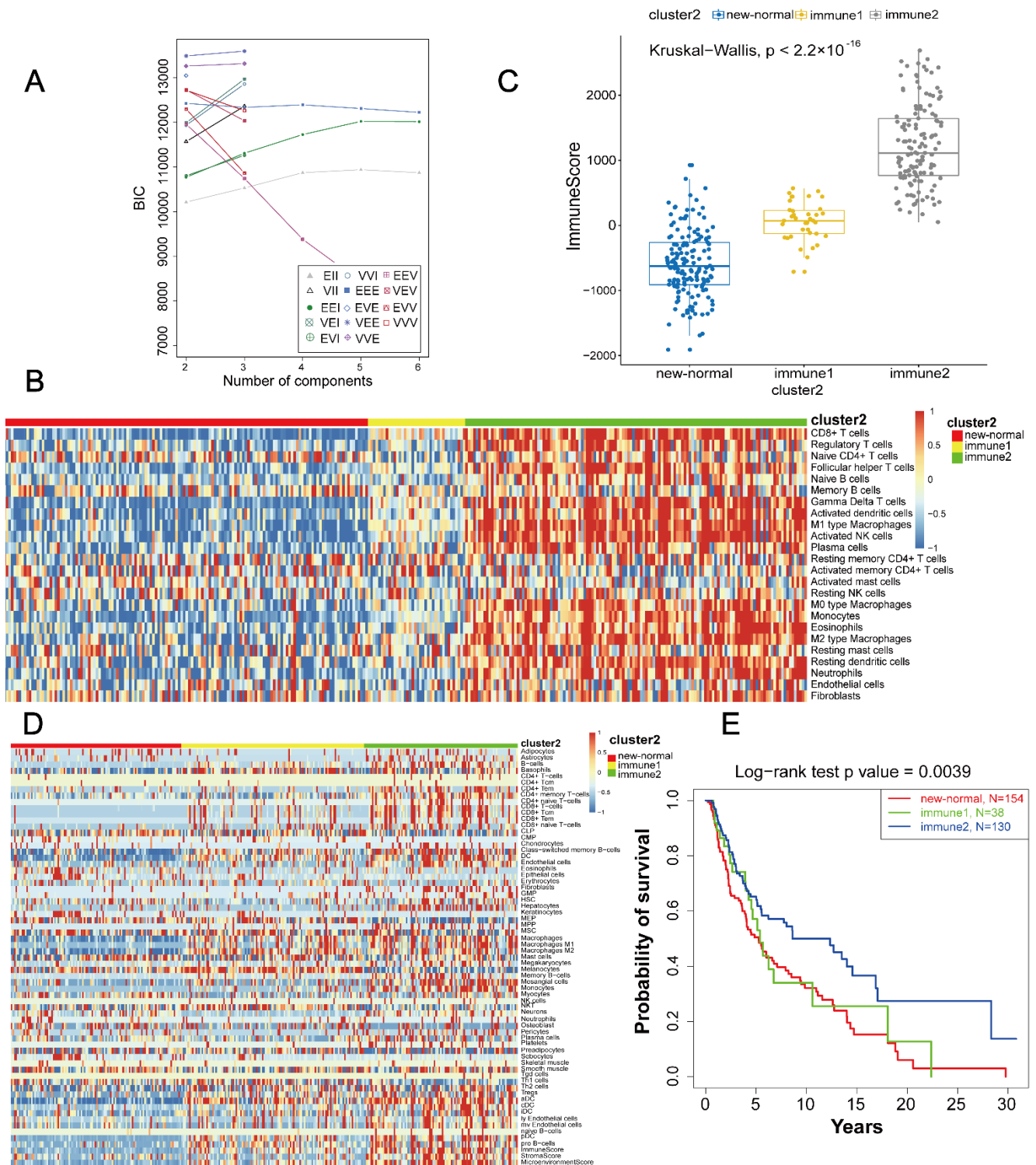


**Figure 3.** Definition and extraction of all subtypes. (A) Determination of the optimal clustering number in immune type according to BIC values ( $k = 3$ ). (B) Heatmap of tumour microenvironment in three subtypes. (C) Significantly different immune scores among the three subtypes ( $p < 2.2 \times 10^{-16}$ ). (D) xCell immune and stromal cell infiltration abundances in the three subtypes. (E) Immune 2 (“high immune subtype”) had the best survival analysis among the three subtypes ( $p = 0.0039$ ).

Combined with the immune score and survival prognosis of each subtype, we re-named the “new-normal class” the “immune inactivation subtype”, the “immune 1 class” the “low immune subtype” and the “immune 2 class” the “high immune subtype”.

### 3.3. Heterogeneity Analysis between High and Low Immune Subtypes

Based on differential gene expression analysis, the expression of 1030 genes in the “high immune subtype” were significantly upregulated relative to that in the “low immune subtype”, and 87 genes were significantly downregulated (Figure 4A). Compared with the immune cell gene set, 240 genes were found to be immune-related among the significantly upregulated genes in the “high immune subtype”, while only one immune-related gene was significantly downregulated. These results indicate that the “high immune subtype” had more immune-enriched characteristics.

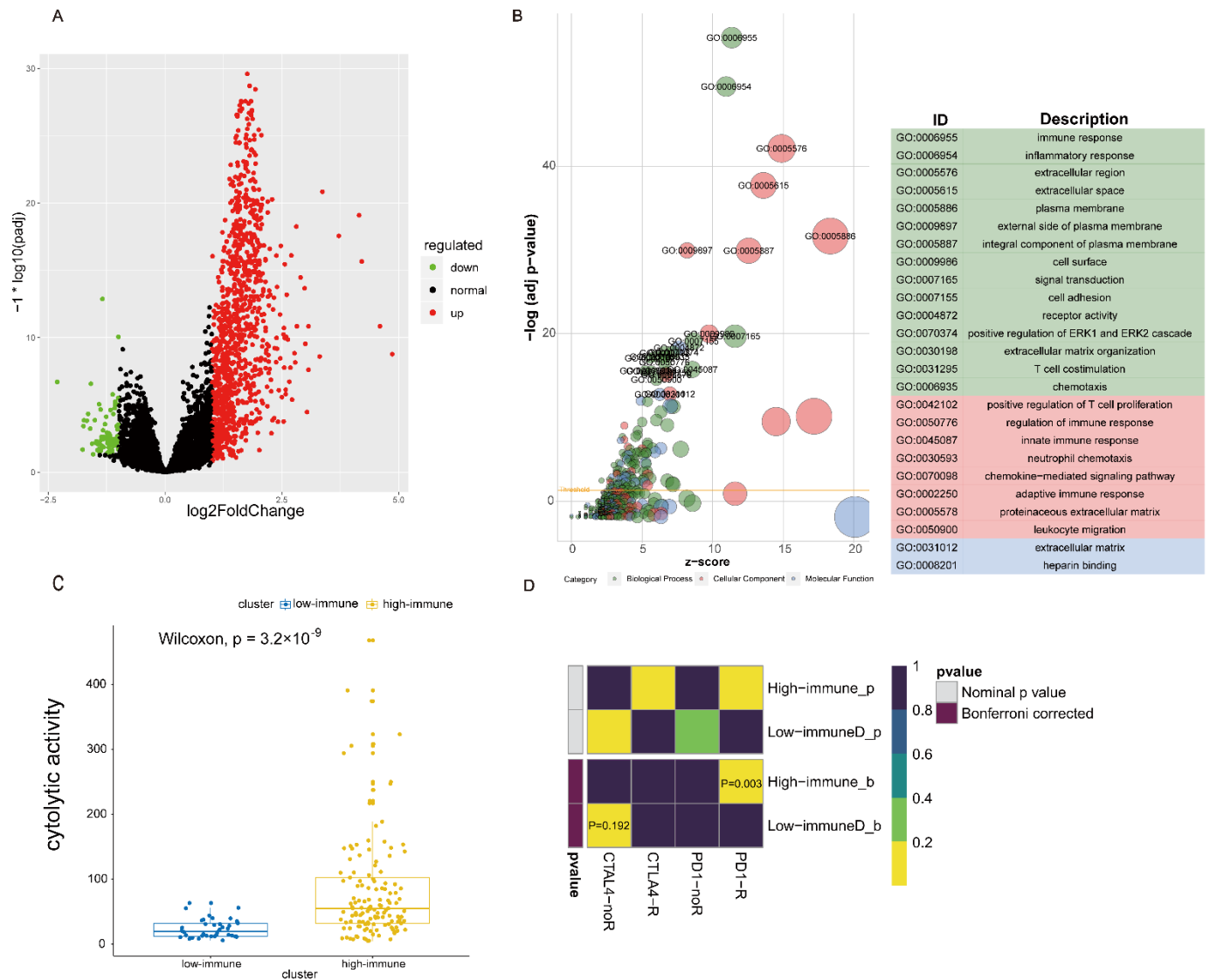


**Figure 4.** Heterogeneity analysis between high and low immune subtypes. **(A)** Volcano plot of differential gene expression in high and low immune subtypes. **(B)** GO functional annotation bubble chart for 1117 DEGs. **(C)** Comparison of cytotoxicity levels in high and low immune subtypes ( $p = 3.2 \times 10^{-9}$ ). **(D)** Submap analysis suggested that the “high immune subtype” might be more sensitive to PD-1 inhibitors (Bonferroni corrected  $p = 0.03$ ).

Based on 1117 differentially expressed genes between the “high immune subtype” and “low immune subtype”, GO functional annotation and KEGG pathway enrichment were further analysed. These differentially expressed genes were mainly related to the immune response, inflammatory response, T cell proliferation, leukocyte proliferation, and chemokine-mediated signalling pathways (Figure 4B). Using KEGG pathway analysis, 16 signalling pathways were identified (Supplementary Table S3). Among those, 13 also appeared in



the normal and immune classes. The PI3K-Akt, MAPK, and TGF- $\beta$  signalling pathways appeared in the enrichment pathway of differentially expressed genes between the “low immune subtype” and “high immune subtype”. Several KEGG pathways were also found to be related to Th1 cell differentiation, Th2 cell differentiation, Th17 cell differentiation, and PD-L1 expression. They showed an increasing trend among the “immune inactivation subtype”, “low immune subtype” and “high immune subtype” (Supplementary Figure S3). There were significant differences (Th1:  $p < 2.2 \times 10^{-16}$ , Th2:  $p = 3.5 \times 10^{-11}$ , Th17:  $p = 4.0 \times 10^{-12}$ ), and the abundance of MDSCs was the highest in the “immune inactivation subtypes” and lowest in the “high immune subtype” ( $p = 9.1 \times 10^{-15}$ ).

The influence and interaction between various factors in the tumour were complex, and the methylation status and gene mutations in the tumour had a strong relationship with gene expression, which would affect tumour occurrence and development. Therefore, we continued to explore the differences between the “high immune subtype” and “low immune subtype” based on tumour methylation and gene mutation. In this study, 21,981 probes were screened for methylation differences between high and low immune subtypes; 982 probes were hypermethylated, and 4620 probes were demethylated. After mapping these probes to genes and annotating with immune gene sets, a total of 597 genes showed hypermethylation but were epigenetically silenced in the “high immune subtype”, among which 10 genes were immune system related. In addition, 1490 genes were demethylated, of which 60 were related to immunity. Then, six significantly mutated genes were identified with a  $p$ -value  $< 0.01$ , including *NRAS*, *BRAF*, *B2M*, *PTEN*, *TP53*, and *CDKN2A* (Supplementary Figure S4). *NRAS* appeared in both the “high immune subtype” and the “low immune subtype”. In addition, *BRAF* and *CDKN2A*, which are star mutations in SKCM [46], appeared in the “high immune subtype”, and the mutation frequency of *BRAF* in the “high immune subtype” was greatest. *BRAF* is commonly seen in the MAPK pathway (RAS/RAF/MEK/ERK pathway), and mutation of this pathway is an important factor that causes growth and development of melanoma. These results indicate that *NRAS* and *BRAF* mutations were specific characteristics of the two subtypes. Additionally, *B2M* and *PTEN* mutations occurred only in the “immune inactivation subtype”.

There were no significant differences in TMB levels between the “high immune subtype” and “low immune subtype”. Because the TMB level of the “immune class” was significantly higher than that of the “normal class” ( $p = 0.00058$ ; Supplementary Figure S5), we suggested that the immune class was more likely to benefit from immunotherapy. Moreover, the “high immune subtype” was more promising for PD-1 treatment [45] (Bonferroni correction  $p = 0.03$ ; Figure 4D). Cell cytotoxicity and cytolysis are also markers of tumour immunogenicity. The cytotoxicity and cytolysis of the “high immune subtype” was significantly higher than that of the “low immune subtype” ( $p = 3.2 \times 10^{-9}$ ; Figure 4C).

### 3.4. Immunity Subtype Validation

In this study, four independent cohorts were integrated as a verification set for supervised analysis (206 tumour samples). First, the existence of an immune class (Cluster 1) and a normal class (Cluster 2) were verified, with the immune class having higher immune signatures (Supplementary Figure S6). To further validate immune subtypes based on the tumour microenvironment, three subtypes of the TCGA cohort were analysed for pairwise differential expression, and the corresponding differentially expressed genes were selected as the specific signatures of the three SKCM immune subtypes. Among them, a 737-gene signature was identified for “immune inactivation subtypes”, a 525-gene signature for “low immune subtype”, and an 839-gene signature for “high immune subtype”. Using the above characterization gene signatures for supervised consensus clustering (Figure 5A), three subtypes of the validation cohort were reproduced: “high immune subtype” (98 samples), “low immune subtype” (58 samples), and “immune inactivation subtypes” (50 samples). Among the three subtypes, significant differences were observed in cell cytotoxicity and cytolysis, immune score, and stromal score (Figure 5B–D,  $p < 0.05$ ).

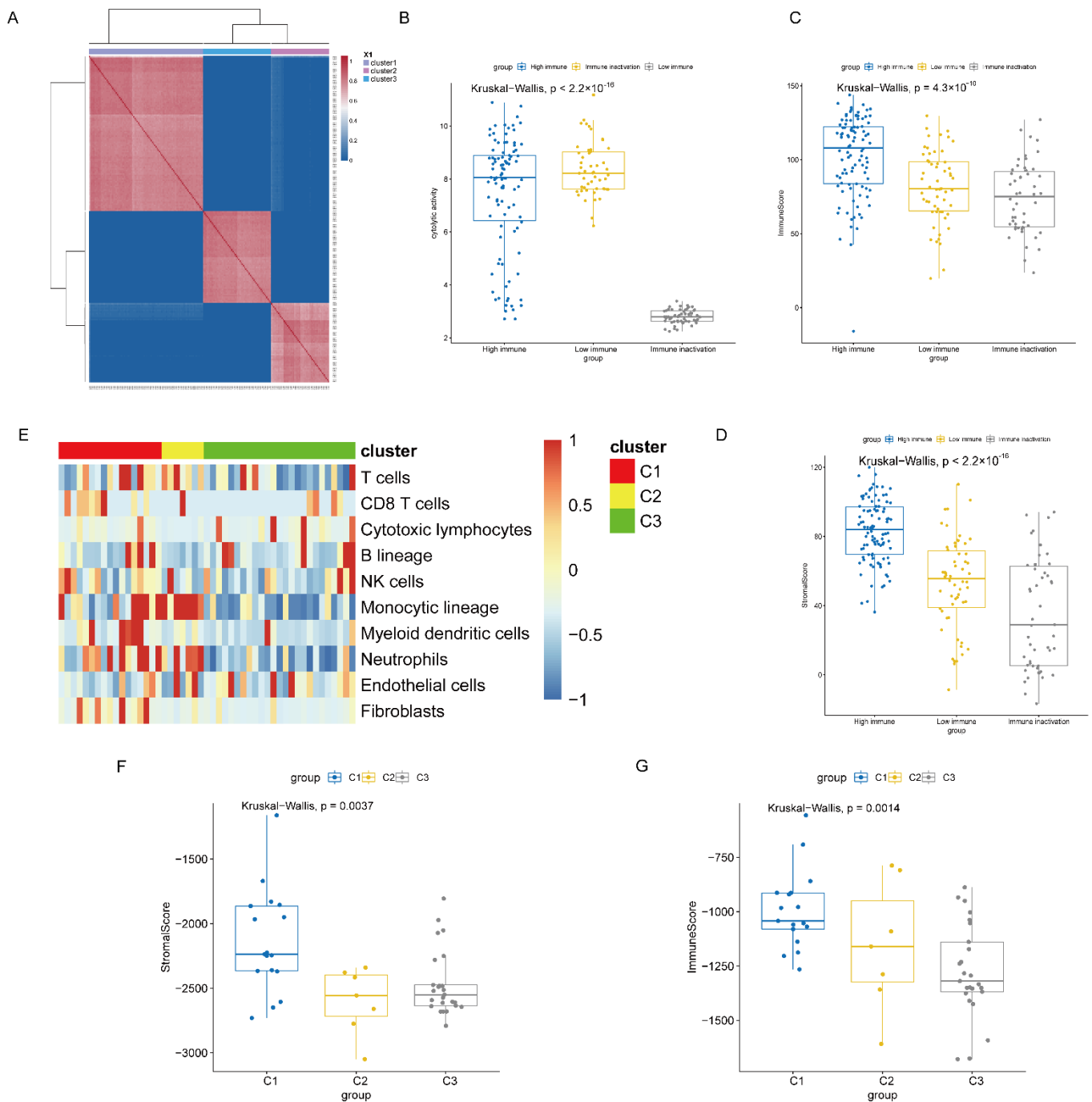


**Figure 5.** Identifications of “high immune subtype”, “low immune subtype”, and “immune inactivation subtype”. (A) Consensus clustering by using three gene signatures on validation sets. (B–D) Significant differences among the three subtypes were found in cell cytotoxicity and cytolysis, immune score, and stromal score (all,  $p < 0.05$ ). (E–G) Significant differences among the three clusters in cell lines were found in tumour microenvironment, immune score, and stromal score (all,  $p < 0.05$ ).

Then, we validated the results on cell lines of cutaneous melanoma. We applied the SING method on the cell lines data ( $n = 49$ ), the optimal clustering number was three according to the BIC value (Supplementary Figure S7). Comparing the tumour microenvironment, stromal score, and immune score of the three clusters (Figure 5E–G,  $p < 0.05$ ), we found significant differences among them. Tumour immune infiltration in the “C1” was significantly higher than that in the other two clusters, which was highly similar

to the “high immune subtype”. However, cytolytic activity score among three clusters were not significant as the expressions of the cell lines were too low (Supplementary Figure S7). Above all, these results suggested that specific immune subtypes were present in cutaneous melanoma and that their immune responses varied according to subtype characteristics in tumour samples and cell lines.

### 3.5. Specific Pathological and Prognostic Features of Immune Subtypes

For 327 samples, the heterogeneity in clinical features among the three immune subtypes was explored from the following six perspectives (Table 1): (1) age, (2) tumour registration, (3) race, (4) body mass index (BMI), (5) metastatic status, and (6) UV exposure rate. We did not observe differences in age, race, BMI, or UV exposure rates among subtypes, but significant differences were found in tumour grade and tumour status ( $p < 0.05$ ). Specifically, more tumour grade samples were III or IV in the “high immune subtype” (“immune inactivation subtype” vs. “low immune subtype” vs. “high immune subtype”: 37% vs. 37% vs. 50%,  $p = 0.05$ ), and the proportion of metastatic samples was higher (“immune inactivation subtype” vs. “low immune subtype” vs. “high immune subtype”: 69% vs. 87% vs. 94%,  $p = 6.21 \times 10^{-8}$ ).

**Table 1.** Statistics of pathological characteristics of immune subtypes and differences among three subtypes.

KERRYPNX	FRE (%)	Specific Immune Subtype			p-Value
		Immune in Activation Subtype	Low Immune Subtype	High Immune Subtype	
Age	≤60	179 (55)	79	23	0.64
	>60	144 (44)	75	15	
	NA	4 (1)	2	0	
TNM Stage	0 + I + II	163 (50)	89	21	0.05
	III + IV	137 (42)	57	14	
	NA	27 (8)	10	3	
Race	White	318 (97)	150	37	0.43
	Asians	7 (2)	5	1	
	Black or African American	1 (0)	0	0	
	NA	1 (0)	1	0	
BMI	≤25	46 (14)	27	5	0.52
	>25	90 (28)	42	12	
	NA	191 (58)	87	21	
Tumour Status	Primary	62 (19)	49	5	$6.214 \times 10^{-8} *$
	Metastatic	265 (81)	107	33	
UV Exposure Rate	≤0.8	83 (25)	47	11	0.07
	>0.8	244 (75)	109	27	

\* Fisher’s exact test  $p$ -value  $< 0.05$ .

We calculated the risk score using a multivariate Cox regression model. Based on the eight-immune-related genes (IRGs) signature (*PSME*, *CDC42*, *CMTM6*, *HLA-DQB1*, *HLA-C*, *CXCR6*, *CD8B*, *TNFSF13*) and the five-immune-associated gene (IAG) signature (*IFITM1*, *TNFSF13B*, *APOBEC3G*, *CCL8*, and *KLRK1*), both published signatures [43,44] showed prognostic value when reproducing them in our study ( $p < 0.001$ , HR = 1.765, 95% CI: 1.297–2.402;  $p = 0.0667$ , HR = 1.328, 95% CI: 0.9807–1.797). Additionally, we found

significant differences in the risk score between the three immune subtypes ( $p < 0.05$ ). Among them (Supplementary Figure S8), “high immune subtype” had a lower risk score, suggesting that “high immune subtype” may have a better prognosis, lower tumour purity and active immune-related signalling pathways.

#### 4. Discussion

In recent years, research on tumour immunotherapy has made rapid progress, and immunotherapy led by SKCM has received extensive attention [18]. At present, molecular typing based on immune function is considered an effective method to improve the efficacy of tumour immunotherapy [47] because it can identify people with specific biological characteristics for valuable treatment. The construction of a sample gene network [48] can help to characterize complex and heterogeneous multigroup data sets and improve the accuracy of subtype identification and subsequent analysis. LIONESS and PAN [14–16] have already been proven to identify subgroups of different disease types and to solve clinically related classification problems.

We herein started by considering the tumour microenvironment and tumour cells and built the SING method by immune annotation information as background to explore the immune function of cutaneous melanoma-related subtypes of skin. The SING algorithm is helpful to identify immune functions related to subtypes. The “immune inactivation subtype” had two unique genetic mutations, *B2M* and *PTEN*, which meant that they were molecular features of the normal class. Studies have found that *B2M* is associated with antigen presentation in the tumour immune cycle [49]. *B2M* gene-encoded  $\beta$ -20 microglobulin (MHC-1) is an important adjunct to major histocompatibility complex class 1, and its absence leads to a decline in MHC-1 expression, affecting antigen presentation and resulting in PD-1 drug resistance [50]. A meta-analysis to systematically review [51] showed that PD-1 inhibitors significantly improved the progression-free survival (PFS), overall survival (OS) and overall response rate (ORR) in patients with advanced melanoma. Anti-PD-1 drugs such as pembrolizumab and nivolumab can achieve long-term survival for patients with metastatic melanoma [52]. *PTEN*, as a tumour suppressor gene [53], was found only in the normal class, suggesting that *PTEN* mutations may be a factor affecting immune properties. Therefore, we suggest that they are potential therapeutic targets to improve the immune response. Compared with the “low immune subtype”, “high immune subtype” showed higher immune infiltration and immune activation characteristics and was significantly enriched in TGF- $\beta$  signalling pathways [54,55]. TGF- $\beta$  signalling pathways have been repeatedly reported [54,56,57] to be associated with immune regulation, and the use of TGF- $\beta$  inhibitors may improve the immune response to immunotherapy. In recent years, inhibitors targeting TGF- $\beta$  pathway have been discovered and investigated by pharmaceutical companies for cancer therapy, and some of them are in clinical trial now, such as Phase I study of GC1008 (fresolimumab), Ph II study of NCT01453361 (Gemogenovatucel-T) and so on [58,59]. In 2019, Kaczorowski et al. [60] suggested that overexpression of SMAD7 may be a new hallmark inhibitor of TGF- $\beta$  in melanoma. In 2021, Liu et al. [61] proposed a triple combination therapy with PD-1/PD-L1, *BRAF*, and *MEK* inhibitor in stage III-IV melanoma as significantly improving PFS of patients. Based on the risk score between the three immune subtypes, “high immune subtype” showed better prognostic value. Therefore, we speculated that patients with “high immune subtype” biological characteristics can generally obtain a better immune prognosis and that the immune prognosis is improved if combined with TGF- $\beta$  inhibitors. In the “low immune subtype”, only one significantly mutated gene, *NRAS*, was found, which was considered a molecular feature of this subtype.

Although we divided the immune subtypes of cutaneous melanoma from the effects of tumour cells and the tumour microenvironment, there were still some inextricable links among various factors that we did not consider. We also have not considered the interaction between factors from comprehensive perspectives. Not with-standing its limitation, this study does suggest that the research of cancer typing based on immune function can be

enhanced by using a sample-specific network. Further study is needed on how to combine the key factors that influence the response to cancer and treatment to conduct a complete analysis of cancer.

## 5. Conclusions

In summary, this comprehensive study classified cutaneous melanoma skin samples based on immune function and proposed three subtypes according to SING and the tumour microenvironment. Mutations in *B2M* and *PTEN* are considered potential therapeutic targets that can improve the immune response. “High immune subtype” patients can generally obtain a better immune prognosis effect if TGF- $\beta$  inhibitors are combined.

**Supplementary Materials:** The following are available online at <https://www.mdpi.com/article/10.3390/life11090925/s1>.

**Author Contributions:** Conceptualization, Conception, and design: F.Y., B.J.; administrative support: F.Y., B.J.; collection and assembly of data: L.L., T.J., J.Z. and M.H.; data analysis and interpretation: L.L., T.J., J.Z., M.H., Y.C., L.X. and W.C.; manuscript writing: all authors; final approval of manuscript: All authors. All authors have read and agreed to the published version of the manuscript.

**Funding:** This work was supported by the National Key R&D Program of China (2019YFC1711000), the National Natural Science Foundation of China (81973145), Key R&D Program of Jiangsu Province [Social Development] (BE2020694).

**Institutional Review Board Statement:** Not applicable.

**Informed Consent Statement:** Not applicable.

**Data Availability Statement:** Raw data for this study were generated at TCGA with cancer type of SKCM. The datasets used and/or analyzed during the current study are available from GEO database (GSE7553, GSE23376, GSE19234, GSE15605).

**Acknowledgments:** The results published here are based upon data generated by TCGA and GEO. We are grateful to patients and investigators who participated in TCGA and GEO for providing data.

**Conflicts of Interest:** The authors declare that the research was conducted in the absence of any commercial or financial relationships that could be construed as a potential conflict of interest.

## References

- Dai, X.; Li, T.; Bai, Z.; Yang, Y.; Liu, X.; Zhan, J.; Shi, B. Breast cancer intrinsic subtype classification, clinical use and future trends. *Am. J. Cancer Res.* **2015**, *5*, 2929–2943.
- Gendoo, D.M.; Ratanasirigulchai, N.; Schroder, M.S.; Pare, L.; Parker, J.S.; Prat, A.; Haibe-Kains, B. Genefu: An R/Bioconductor package for computation of gene expression-based signatures in breast cancer. *Bioinformatics* **2016**, *32*, 1097–1099. [[CrossRef](#)] [[PubMed](#)]
- Beattie, J.; Yarmus, L.; Wahidi, M.; Rivera, M.P.; Gilbert, C.; Maldonado, F.; Czarnecka, K.; Argento, A.; Chen, A.; Herth, F.; et al. The Immune Landscape of Non-Small-Cell Lung Cancer. Utility of Cytologic and Histologic Samples Obtained through Minimally Invasive Pulmonary Procedures. *Am. J. Respir. Crit. Care Med.* **2018**, *198*, 24–38. [[CrossRef](#)] [[PubMed](#)]
- Dagogo-Jack, I.; Shaw, A.T. Tumour heterogeneity and resistance to cancer therapies. *Nat. Rev. Clin. Oncol.* **2018**, *15*, 81–94. [[CrossRef](#)]
- Guo, W.F.; Zhang, S.W.; Liu, L.L.; Liu, F.; Shi, Q.Q.; Zhang, L.; Tang, Y.; Zeng, T.; Chen, L. Discovering personalized driver mutation profiles of single samples in cancer by network control strategy. *Bioinformatics* **2018**, *34*, 1893–1903. [[CrossRef](#)] [[PubMed](#)]
- Wang, H.; Sun, Q.; Zhao, W.; Qi, L.; Gu, Y.; Li, P.; Zhang, M.; Li, Y.; Liu, S.L.; Guo, Z. Individual-level analysis of differential expression of genes and pathways for personalized medicine. *Bioinformatics* **2015**, *31*, 62–68. [[CrossRef](#)]
- Yu, X.; Zhang, J.; Sun, S.; Zhou, X.; Zeng, T.; Chen, L. Individual-specific edge-network analysis for disease prediction. *Nucleic Acids Res.* **2017**, *45*, e170. [[CrossRef](#)] [[PubMed](#)]
- Gnant, M.; Harbeck, N.; Thomssen, C. St. Gallen/Vienna 2017: A Brief Summary of the Consensus Discussion about Escalation and De-Escalation of Primary Breast Cancer Treatment. *Breast Care* **2017**, *12*, 102–107. [[CrossRef](#)]
- Liu, X.P.; Wang, Y.T.; Ji, H.B.; Aihara, K.; Chen, L.N. Personalized characterization of diseases using sample-specific networks. *Nucleic Acids Res.* **2016**, *44*, e164. [[CrossRef](#)]
- Wayteck, L.; Breckpot, K.; Demeester, J.; De Smedt, S.C.; Raemdonck, K. A personalized view on cancer immunotherapy. *Cancer Lett.* **2014**, *352*, 113–125. [[CrossRef](#)]

11. Balaguer, M.A.D.; Fisher, A.P.; Clark, N.M.; Fernandez-Espinosa, M.G.; Moller, B.K.; Weijers, D.; Lohmann, J.U.; Williams, C.; Lorenzo, O.; Sozzani, R. Predicting gene regulatory networks by combining spatial and temporal gene expression data in Arabidopsis root stem cells. *Proc. Natl. Acad. Sci. USA* **2017**, *114*, E7632–E7640. [[CrossRef](#)]
12. Qiu, X.; Rahimzamani, A.; Wang, L.; Mao, Q.; Durham, T.; McFaline-Figueroa, J.L.; Saunders, L.; Trapnell, C.; Kannan, S. Towards inferring causal gene regulatory networks from single cell expression Measurements. *bioRxiv* **2018**, *10*, 426981. [[CrossRef](#)]
13. Liu, Z.P.; Wu, H.; Zhu, J.; Miao, H. Systematic identification of transcriptional and post-transcriptional regulations in human respiratory epithelial cells during influenza A virus infection. *BMC Bioinform.* **2014**, *15*, 336. [[CrossRef](#)]
14. Borgwardt, K.M.; Kriegel, H.P.; Vishwanathan, S.V.; Schraudolph, N.N. Graph kernels for disease outcome prediction from protein-protein interaction networks. In *Biocomputing 2007*; World Scientific: Singapore, 2006; pp. 4–15. [[CrossRef](#)]
15. Kuijjer, M.L.; Tung, M.G.; Yuan, G.; Quackenbush, J.; Glass, K. Estimating Sample-Specific Regulatory Networks. *iScience* **2019**, *14*, 226–240. [[CrossRef](#)]
16. Nguyen, T.; Lee, S.C.; Quinn, T.P.; Truong, B.; Li, X.; Tran, T.; Venkatesh, S.; Le, T.D. PAN: Personalized Annotation-based Networks for the Prediction of Breast Cancer Relapse. In *IEEE/ACM Transactions on Computational Biology and Bioinformatics*; IEEE: Piscataway, NJ, USA, 2021. [[CrossRef](#)]
17. Chi, Z.; Li, S.; Sheng, X.; Si, L.; Cui, C.; Han, M.; Guo, J. Clinical presentation, histology, and prognoses of malignant melanoma in ethnic Chinese: A study of 522 consecutive cases. *BMC Cancer* **2011**, *11*, 85. [[CrossRef](#)] [[PubMed](#)]
18. Leonardi, G.C.; Falzone, L.; Salemi, R.; Zanghi, A.; Spandidos, D.A.; McCubrey, J.A.; Candido, S.; Libra, M. Cutaneous melanoma: From pathogenesis to therapy (Review). *Int. J. Oncol.* **2018**, *52*, 1071–1080. [[CrossRef](#)]
19. Davis, L.E.; Shalin, S.C.; Tackett, A.J. Current state of melanoma diagnosis and treatment. *Cancer Biol. Ther.* **2019**, *20*, 1366–1379. [[CrossRef](#)] [[PubMed](#)]
20. Erdag, G.; Schaefer, J.T.; Smolkin, M.E.; Deacon, D.H.; Shea, S.M.; Dengel, L.T.; Patterson, J.W.; Slingluff, C.L., Jr. Immunotype and immunohistologic characteristics of tumor-infiltrating immune cells are associated with clinical outcome in metastatic melanoma. *Cancer Res.* **2012**, *72*, 1070–1080. [[CrossRef](#)] [[PubMed](#)]
21. Marra, A.; Ferrone, C.R.; Fuscillo, C.; Scognamiglio, G.; Ferrone, S.; Pepe, S.; Perri, F.; Sabbatino, F. Translational Research in Cutaneous Melanoma: New Therapeutic Perspectives. *Anticancer. Agents Med. Chem.* **2018**, *18*, 166–181. [[CrossRef](#)]
22. Riker, A.I.; Enkemann, S.A.; Fodstad, O.; Liu, S.H.; Ren, S.P.; Morris, C.; Xi, Y.G.; Howell, P.; Metge, B.; Samant, R.S.; et al. The gene expression profiles of primary and metastatic melanoma yields a transition point of tumor progression and metastasis. *BMC Med. Genom.* **2008**, *1*, 13. [[CrossRef](#)]
23. Holtan, S.G.; Mansfield, A.S.; Creedon, D.J.; Nevala, W.K.; Haluska, P.; Leontovich, A.A.; Markovic, S.N. An organ system based approach to prognosis in advanced melanoma. *Front. Biosci. Elite. Ed.* **2012**, *4*, 2723–2733. Available online: <https://www.ncbi.nlm.nih.gov/geo/query/acc.cgi?acc=GSE23376> (accessed on 1 July 2021).
24. Bogunovic, D.; O'Neill, D.W.; Belitskaya-Levy, I.; Vacic, V.; Yu, Y.L.; Adams, S.; Darvishian, F.; Berman, R.; Shapiro, R.; Pavlick, A.C.; et al. Immune profile and mitotic index of metastatic melanoma lesions enhance clinical staging in predicting patient survival. *Proc. Natl. Acad. Sci. USA* **2009**, *106*, 20429–20434. [[CrossRef](#)]
25. Raskin, L.; Fullen, D.R.; Giordano, T.J.; Thomas, D.G.; Frohm, M.L.; Cha, K.B.; Ahn, J.; Mukherjee, B.; Johnson, T.M.; Gruber, S.B. Transcriptome Profiling Identifies HMGA2 as a Biomarker of Melanoma Progression and Prognosis. *J. Investig. Derm.* **2013**, *133*, 2585–2592. [[CrossRef](#)]
26. Ghandi, M.; Huang, F.W.; Jane-Valbuena, J.; Kryukov, G.V.; Lo, C.C.; McDonald, E.R., 3rd; Barretina, J.; Gelfand, E.T.; Bielski, C.M.; Li, H.; et al. Next-generation characterization of the Cancer Cell Line Encyclopedia. *Nature* **2019**, *569*, 503–508. [[CrossRef](#)]
27. The Cancer Genome Atlas Research Network. Comprehensive molecular characterization of urothelial bladder carcinoma. *Nature* **2014**, *507*, 315–322. [[CrossRef](#)] [[PubMed](#)]
28. Becht, E.; Giraldo, N.A.; Lacroix, L.; Buttard, B.; Elarouci, N.; Petitprez, F.; Selves, J.; Laurent-Puig, P.; Sautes-Fridman, C.; Fridman, W.H.; et al. Estimating the population abundance of tissue-infiltrating immune and stromal cell populations using gene expression. *Genome Biol.* **2016**, *17*, 218. [[CrossRef](#)]
29. Aran, D.; Hu, Z.; Butte, A.J. xCell: Digitally portraying the tissue cellular heterogeneity landscape. *Genome Biol.* **2017**, *18*, 220. [[CrossRef](#)] [[PubMed](#)]
30. Yoshihara, K.; Shahmoradgoli, M.; Martinez, E.; Vegesna, R.; Kim, H.; Torres-Garcia, W.; Trevino, V.; Shen, H.; Laird, P.W.; Levine, D.A.; et al. Inferring tumour purity and stromal and immune cell admixture from expression data. *Nat. Commun.* **2013**, *4*, 2612. [[CrossRef](#)] [[PubMed](#)]
31. Rooney, M.S.; Shukla, S.A.; Wu, C.J.; Getz, G.; Hacohen, N. Molecular and Genetic Properties of Tumors Associated with Local Immune Cytolytic Activity. *Cell* **2015**, *160*, 48–61. [[CrossRef](#)]
32. Anders, S.; Huber, W. Differential expression analysis for sequence count data. *Genome Biol.* **2010**, *11*, R106. [[CrossRef](#)]
33. Dennis, G., Jr.; Sherman, B.T.; Hosack, D.A.; Yang, J.; Gao, W.; Lane, H.C.; Lempicki, R.A. DAVID: Database for Annotation, Visualization, and Integrated Discovery. *Genome Biol.* **2003**, *4*, r60. [[CrossRef](#)]
34. Huang, D.W.; Sherman, B.T.; Lempicki, R.A. Systematic and integrative analysis of large gene lists using DAVID bioinformatics resources. *Nat. Protoc.* **2009**, *4*, 44–57. [[CrossRef](#)]
35. Yu, G.C.; Wang, L.G.; Han, Y.Y.; He, Q.Y. clusterProfiler: An R Package for Comparing Biological Themes Among Gene Clusters. *Omics A J. Integr. Biol.* **2012**, *16*, 284–287. [[CrossRef](#)]

36. Hanzelmann, S.; Castelo, R.; Guinney, J. GSEA: Gene set variation analysis for microarray and RNA-Seq data. *BMC Bioinform.* **2013**, *14*, 7. [[CrossRef](#)]
37. Lawrence, M.S.; Stojanov, P.; Polak, P.; Kryukov, G.V.; Cibulskis, K.; Sivachenko, A.; Carter, S.L.; Stewart, C.; Mermel, C.H.; Roberts, S.A.; et al. Mutational heterogeneity in cancer and the search for new cancer-associated genes. *Nature* **2013**, *499*, 214–218. [[CrossRef](#)] [[PubMed](#)]
38. Steuer, C.E.; Ramalingam, S.S. Tumor Mutation Burden: Leading Immunotherapy to the Era of Precision Medicine? *J. Clin. Oncol.* **2018**, *36*, 631–632. [[CrossRef](#)] [[PubMed](#)]
39. Morris, T.J.; Butcher, L.M.; Feber, A.; Teschendorff, A.E.; Chakravarthy, A.R.; Wojdacz, T.K.; Beck, S. ChAMP: 450k Chip Analysis Methylation Pipeline. *Bioinformatics* **2014**, *30*, 428–430. [[CrossRef](#)] [[PubMed](#)]
40. Bland, J.M.; Altman, D.G. Statistics notes—Survival probabilities (the Kaplan-Meier method). *Bri. Med. J.* **1998**, *317*, 1572. [[CrossRef](#)]
41. Zhang, M.J. Cox proportional hazards regression models for survival data in cancer research. *Cancer Treat. Res.* **2002**, *113*, 59–70. [[CrossRef](#)]
42. Roemeling, S.; Roobol, M.J.; Kattan, M.W.; van der Kwast, T.H.; Steyerberg, E.W.; Schroder, F.H. Nomogram use for the prediction of indolent prostate cancer—Impact on screen-detected populations. *Cancer Am. Cancer Soc.* **2007**, *110*, 2218–2221. [[CrossRef](#)]
43. Huang, R.; Mao, M.; Lu, Y.; Yu, Q.; Liao, L. A novel immune-related genes prognosis biomarker for melanoma: Associated with tumor microenvironment. *Aging* **2020**, *12*, 6966–6980. [[CrossRef](#)]
44. Hu, B.; Wei, Q.; Zhou, C.; Ju, M.; Wang, L.; Chen, L.; Li, Z.; Wei, M.; He, M.; Zhao, L. Analysis of immune subtypes based on immunogenomic profiling identifies prognostic signature for cutaneous melanoma. *Int. Immunopharmacol.* **2020**, *89*, 107162. [[CrossRef](#)] [[PubMed](#)]
45. Roh, W.; Chen, P.L.; Reuben, A.; Spencer, C.N.; Prieto, P.A.; Miller, J.P.; Gopalakrishnan, V.; Wang, F.; Cooper, Z.A.; Reddy, S.M.; et al. Integrated molecular analysis of tumor biopsies on sequential CTLA-4 and PD-1 blockade reveals markers of response and resistance. *Sci. Transl. Med.* **2017**, *9*, eaah3560. [[CrossRef](#)]
46. Zeng, H.L.; Jorapur, A.; Shain, A.H.; Lang, U.E.; Torres, R.; Zhang, Y.T.; McNeal, A.S.; Botton, T.; Lin, J.; Donne, M.; et al. Bi-allelic Loss of CDKN2A Initiates Melanoma Invasion via BRN2 Activation. *Cancer Cell* **2018**, *34*, 56–68. [[CrossRef](#)]
47. Chen, W.Z.; Cheng, P.; Jiang, J.X.; Ren, Y.Q.; Wu, D.; Xue, D. Epigenomic and genomic analysis of transcriptome modulation in skin cutaneous melanoma. *Aging* **2020**, *12*, 12703–12725. [[CrossRef](#)]
48. Lee, W.; Huang, D.S.; Han, K. Constructing cancer patient-specific and group-specific gene networks with multi-omics data. *BMC Med. Genom.* **2020**, *13*, 81. [[CrossRef](#)]
49. Rodig, S.J.; Gusenleitner, D.; Jackson, D.G.; Gjini, E.; Giobbie-Hurder, A.; Jin, C.; Chang, H.; Lovitch, S.B.; Horak, C.; Weber, J.S.; et al. MHC proteins confer differential sensitivity to CTLA-4 and PD-1 blockade in untreated metastatic melanoma. *Sci. Transl. Med.* **2018**, *10*, aar3342. [[CrossRef](#)] [[PubMed](#)]
50. Zaretsky, J.M.; Garcia-Diaz, A.; Shin, D.S.; Escuin-Ordinas, H.; Hugo, W.; Hu-Lieskovan, S.; Torrejon, D.Y.; Abril-Rodriguez, G.; Sandoval, S.; Barthly, L.; et al. Mutations Associated with Acquired Resistance to PD-1 Blockade in Melanoma. *N. Engl. J. Med.* **2016**, *375*, 819–829. [[CrossRef](#)] [[PubMed](#)]
51. Li, J.; Gu, J. Efficacy and safety of PD-1 inhibitors for treating advanced melanoma: A systematic review and meta-analysis. *Immunotherapy* **2018**, *10*, 1293–1302. [[CrossRef](#)]
52. Gellrich, F.F.; Schmitz, M.; Beissert, S.; Meier, F. Anti-PD-1 and Novel Combinations in the Treatment of Melanoma—An Update. *J. Clin. Med.* **2020**, *9*, 223. [[CrossRef](#)]
53. Sana, G.; Madigan, J.P.; Gartner, J.J.; Fourrez, M.; Lin, J.; Qutob, N.; Narayan, J.; Shukla, S.; Ambudkar, S.V.; Xia, D.; et al. Exome Sequencing of ABCB5 Identifies Recurrent Melanoma Mutations that Result in Increased Proliferative and Invasive Capacities. *J. Invest. Dermatol.* **2019**, *139*, 1985–1992. [[CrossRef](#)]
54. Batlle, E.; Massague, J. Transforming Growth Factor-beta Signaling in Immunity and Cancer. *Immunity* **2019**, *50*, 924–940. [[CrossRef](#)]
55. Zaiatz-Bittencourt, V.; Finlay, D.K.; Gardiner, C.M. Canonical TGF-beta Signaling Pathway Represses Human NK Cell Metabolism. *J. Immunol.* **2018**, *200*, 3934–3941. [[CrossRef](#)] [[PubMed](#)]
56. Yang, L.; Pang, Y.; Moses, H.L. TGF-beta and immune cells: An important regulatory axis in the tumor microenvironment and progression. *Trends Immunol.* **2010**, *31*, 220–227. [[CrossRef](#)] [[PubMed](#)]
57. Travis, M.A.; Sheppard, D. TGF-beta activation and function in immunity. *Annu Rev. Immunol.* **2014**, *32*, 51–82. [[CrossRef](#)] [[PubMed](#)]
58. Huang, C.Y.; Chung, C.L.; Hu, T.H.; Chen, J.J.; Liu, P.F.; Chen, C.L. Recent progress in TGF-beta inhibitors for cancer therapy. *Biomed. Pharm.* **2021**, *134*, 111046. [[CrossRef](#)]
59. Morris, J.C.; Tan, A.R.; Olencki, T.E.; Shapiro, G.L.; Dezube, B.J.; Reiss, M.; Hsu, F.J.; Berzofsky, J.A.; Lawrence, D.P. Phase I study of GC1008 (fresolimumab): A human anti-transforming growth factor-beta (TGFbeta) monoclonal antibody in patients with advanced malignant melanoma or renal cell carcinoma. *PLoS ONE* **2014**, *9*, e90353. [[CrossRef](#)]
60. Kaczorowski, M.; Biecek, P.; Donizy, P.; Pieniazek, M.; Matkowski, R.; Halon, A. SMAD7 is a novel independent predictor of survival in patients with cutaneous melanoma. *Transl. Res.* **2019**, *204*, 72–81. [[CrossRef](#)]
61. Liu, Y.; Zhang, X.L.; Wang, G.Y.; Cui, X.C. Triple Combination Therapy With PD-1/PD-L1, BRAF, and MEK Inhibitor for Stage III-IV Melanoma: A Systematic Review and Meta-Analysis. *Front. Oncol.* **2021**, *11*, 2088. [[CrossRef](#)]